**Table 2.** Slope streaks versus RSL.

| Attribute | Slope streaks | RSL |
|---|---|---|
| Slope albedo | High (>0.25) | Low (<0.2) |
| Contrast | ~10% darker | Up to 40% darker |
| Dust index* | High ($e$ < 0.95) | Low ($e$ > 0.96) |
| Thermal inertia | Low (<100) | 180 to 340 |
| Width | Up to 200 m | Up to 5 m |
| Slope aspect preferences | Varies with regional wind flow (*15*) | Equator-facing in middle latitudes |
| Latitudes; longitudes | Corresponds to dust distribution | 32°S to 48°S; all longitudes |
| Formation $L_S$ | All seasons (*31*) | $L_S$ = 240 to 20 |
| Fading time scale | Years to decades | Months |
| Associated with rocks | No | Yes |
| Associated with channels | No | Yes |
| Abundance on a slope | Up to tens | Up to thousands |
| Regional mineralogy | Mars dust | Variable |
| Formation events | One event per streak or streaks | Incremental growth of each feature |
| Yearly recurrence | No | Yes |

*1350 to 1400 cm$^{-1}$ emissivity ($e$) (SOM).

seasonality to their formation (*31*). The Phoenix lander may have observed droplets of brine on the lander legs (*9*), and perchlorates should form liquids at times (*8*, *32*), but definitive evidence for liquid at the landing site is lacking (*33*).

### References and Notes


1. B. C. Clark, *Icarus* **34**, 645 (1978).
2. G. W. Brass, *Icarus* **42**, 20 (1980).
3. S. W. Squyres *et al.*, *Science* **306**, 1709 (2004).
4. A. Gendrin *et al.*, *Science* **307**, 1587 (2005).
5. M. H. Hecht *et al.*, *Science* **325**, 64 (2009).
6. D. W. G. Sears, J. D. Chittenden, *Geophys. Res. Lett.* **32**, L23203 (2005).
7. T. Altheide, V. Chevrier, C. Nicholson, J. Denson, *Earth Planet. Sci. Lett.* **282**, 69 (2009).
8. M.-P. Zorzano, E. Mateo-Marti, O. Prieto-Ballesteros, S. Osuna, N. Renno, *Geophys. Res. Lett.* **36**, L20201 (2009).
9. N. O. Rennó *et al.*, *J. Geophys. Res.* **114**, E00E03 (2009).
10. D. Möhlmann, K. Thomsen, *Icarus* **212**, 123 (2011).
11. A. S. McEwen *et al.*, *Icarus* **205**, 2 (2010).
12. $L_S$ is the true anomaly of Mars in its orbit around the Sun, measured from the vernal equinox, used as a measure of the season on Mars. $L_S$ = 0 corresponds to the beginning of northern spring; $L_S$ = 180 is the beginning of southern spring. The numbering of Mars years (MYs) was defined to facilitate comparison of data sets across decades and multiple Mars missions; year 1 started on 11 April 1955.
13. Time sequences in animated GIF format are posted at http://hirise.lpl.arizona.edu/sim/. These are stacked cutouts from orthorectified HiRISE images archived (or to be archived within 1 year) in the Planetary Data System.
14. S. L. Murchie *et al.*, *J. Geophys. Res.* **112**, E05S03 (2007).
15. J. J. Wray, S. L. Murchie, S. W. Squyres, F. P. Seelos, L. L. Tornabene, *Geology* **37**, 1043 (2009).
16. D. Baratoux *et al.*, *Icarus* **183**, 30 (2006).
17. A. Kereszturi *et al.*, *Icarus* **207**, 149 (2010).
18. C. J. Hansen *et al.*, *Science* **331**, 575 (2011).
19. P. R. Christensen *et al.*, *Space Sci. Rev.* **110**, 85 (2004).
20. H. Viles *et al.*, *Geophys. Res. Lett.* **37**, L18201 (2010).
21. R. Ulrich, T. Kral, V. Chevrier, R. Pilgrim, L. Roe, *Astrobiology* **10**, 643 (2010).
22. M. Kreslavsky, J. W. Head, *Icarus* **201**, 517 (2009).
23. K. J. Kossacki, W. J. Markiewicz, *Icarus* **210**, 83 (2010).
24. M. M. Osterloo, F. S. Anderson, V. E. Hamilton, B. M. Hynek, *J. Geophys. Res.* **115**, E10012 (2010).
25. M. T. Mellon, W. C. Feldman, T. H. Prettyman, *Icarus* **169**, 324 (2004).
26. J. M. Goldspiel, S. W. Squyres, *Icarus* **211**, 238 (2011).
27. H. Zhang, K. J. Voss, *Appl. Opt.* **45**, 8753 (2006).
28. M. C. Malin, K. S. Edgett, L. V. Posiolova, S. M. McColley, E. Z. Dobrea, *Science* **314**, 1573 (2006).
29. C. M. Dundas, A. S. McEwen, S. Diniega, S. Byrne, S. Martinez-Alonso, *Geophys. Res. Lett.* **37**, L07202 (2010).
30. S. Diniega, S. Byrne, N. T. Bridges, C. M. Dundas, A. S. McEwen, *Geology* **38**, 1047 (2010).
31. C. M. King, N. Schorghofer, K. L. Wagstaff, *Lunar Planet. Sci. Conf.* **41**, 1542 (2010).
32. S. C. Cull *et al.*, *Geophys. Res. Lett.* **37**, L22203 (2010).
33. C. R. Stoker *et al.*, *J. Geophys. Res.* **115**, E00E20 (2010).


**Acknowledgments:** This research was supported by NASA's MRO project; we thank them along with the reviewers. All original data reported in this paper are tabulated in the SOM and archived by NASA's Planetary Data System.

**Supporting Online Material**
www.sciencemag.org/cgi/content/full/333/6043/740/DC1
SOM Text
Figs. S1 to S6
Tables S1 to S5
References (*34–48*)

25 February 2011; accepted 17 June 2011
10.1126/science.1204816

# Reduced Interannual Rainfall Variability in East Africa During the Last Ice Age

**Christian Wolff,[1,2,3] Gerald H. Haug,[3,4]* Axel Timmermann,[5] Jaap S. Sinninghe Damsté,[6,7] Achim Brauer,[1] Daniel M. Sigman,[8] Mark A. Cane,[9] Dirk Verschuren[10]**

Interannual rainfall variations in equatorial East Africa are tightly linked to the El Niño Southern Oscillation (ENSO), with more rain and flooding during El Niño and droughts in La Niña years, both having severe impacts on human habitation and food security. Here we report evidence from an annually laminated lake sediment record from southeastern Kenya for interannual to centennial-scale changes in ENSO-related rainfall variability during the last three millennia and for reductions in both the mean rate and the variability of rainfall in East Africa during the Last Glacial period. Climate model simulations support forward extrapolation from these lake sediment data that future warming will intensify the interannual variability of East Africa's rainfall.

In the tropics, changes in rainfall patterns have severe consequences for millions of people. East Africa, in particular, has in recent years experienced both extreme flooding and severe droughts, with serious impacts on developing economies and wildlife throughout the region (*1*). Seasonality in East African climate is controlled primarily by the biannual migration of the Intertropical Convergence Zone (ITCZ) across the region (*2*) (fig. S1). As a result, equatorial East Africa experiences two climatological rainy seasons (*3*). Dry seasons are windy because of the trade winds that straddle the ITCZ. Interannual variations in the seasonal migration of the East African ITCZ are driven to a large extent by the El Niño Southern Oscillation (ENSO) (*4*) and its related western Indian Ocean sea surface temperature (SST) anomalies (*5*, *6*). El Niño events alter the atmospheric circulation, often generating an equatorial Indian Ocean SST pattern that is warmer in the west and cooler in the east, a configuration sometimes referred to as the positive phase of the Indian Ocean Dipole Mode (*7*). Surface ocean warming in the western Indian Ocean leads to intensification and shifts of the ITCZ, bringing more precipitation to East Africa and weakening the local surface winds (*8*, *9*) (Fig. 1A). El Niño thus tends to enhance East African rainfall indirectly by causing a warming in the western Indian Ocean, even though the direct teleconnection through the atmosphere tends to reduce rainfall (*6*).

Here we provide information on interannual climate variability in East Africa going back to the last ice age, using the annual varve thickness record of sedimentation in Lake Challa (3°19'S, 37°42'E; 880 m above sea level), a freshwater crater lake on the lower east slope of Mount Kilimanjaro (Kenya/Tanzania) (fig. S2). The Lake Challa sediment profile is dominated by thick sequences of fine laminations. These laminated sequences, deposited under anoxic conditions, consist of light-dark couplets that accumulated in the lake over the last 25,000 years (*10*) at a sedimentation rate varying between 0.08 and 7 mm $yr^{-1}$ (fig. S3). The darker layers consist largely of amorphous organic matter derived from phytoplankton and calcite crystals precipitated from the water column, whereas diatom frustules are the dominant constituent of the light layers. In order to refine our interpretation of seasonal layer deposition in Lake Challa, a sediment trap program was initiated in 2006 at an offshore location in the lake. Analysis of the monthly collected sediment trap material confirmed the annual origin of the dark-light couplets, with the light layer deposited during the long dry season (June to October, i.e., centered on the austral winter season) and the dark layer representing the two rainy seasons (November to December and March to May) and the brief intervening dry season (January to February) (fig. S4). Comparison of the thickness of the light and dark layer within a year's couplet indicates that the total varve thickness is controlled by the thickness of the light layer (figs. S5 and S6). Thus, varve thickness mainly reflects the quantity of diatom frustules deposited during the dry season and in particular during April to September.

In southeastern Kenya, the windy season begins in April or May, when the ITCZ moves north across the equator and southerly winds become dominant. These winds, which in the modern climate normally last until late October, combine with seasonally lower insolation to cool the lake surface and deepen the mixed layer of the lake from late June to September. During episodes of high wind stress, convection extends to below 35 m depth (as deep as 40 to 45 m in some years) (fig. S7), making the dissolved nutrients that accumulate over time in the deep lower water column available for phytoplankton growth at the lake surface. Enhanced nutrient availability coinciding with a more turbulent water column promotes diatom blooms (*11*), which are preserved as the light layer in the varves. Therefore, we interpret thick varves to indicate years of longer windy conditions. Conversely, thin varves reflect reduced diatom productivity due to weaker winds, characteristic of years when the ITCZ remains overhead or nearby for a greater fraction of the year. Given the modern control of seasonal ITCZ location on wind and rain in this region (*2*–*4*) and the broad inverse relation between rainfall and windiness at the interannual time scale (fig. S8), thick varves represent windier and thus drier years (fig. S9).

El Niño (La Niña) events are associated with wetter (drier) conditions in East Africa and decreased (increased) surface wind speeds (Fig. 1A and fig. S10). We verified the regional significance of our varve thickness record as an ENSO-ITCZ–sensitive record by comparing the varve thickness data of the last 150 years with an ENSO index and a western Indian Ocean SST index (*12*, *13*) (Fig. 1B). To a remarkable degree, thick varves coincide with La Niña years, and thin varves correspond to El Niño years (fig. S11), which supports our expectations based on the

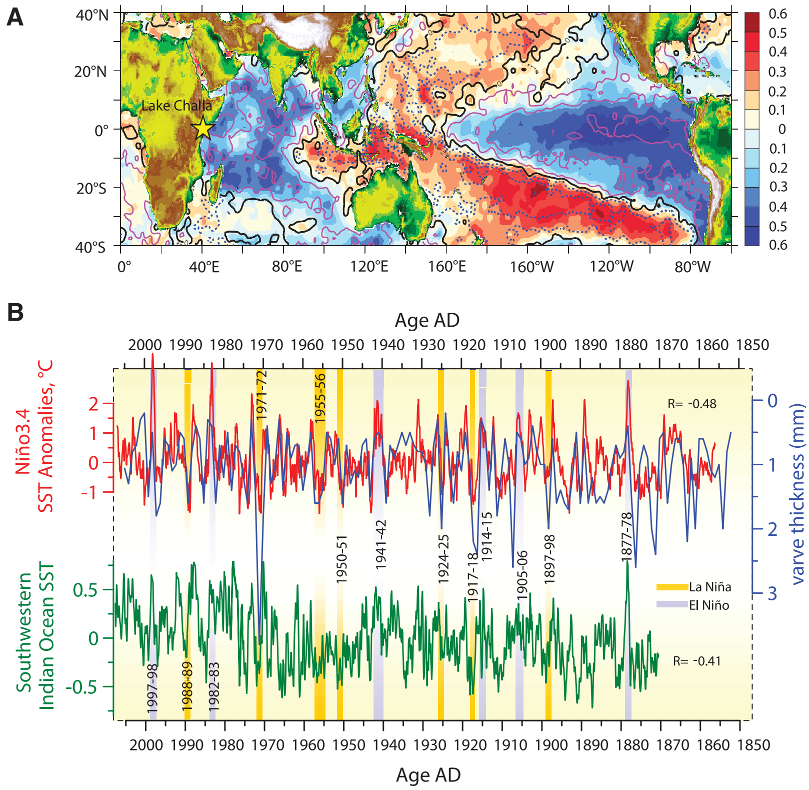


**Fig. 1.** The effect of tropical sea surface temperature anomalies on interannual climate variations in East Africa and varve thickness variations in Lake Challa. (**A**) Shading: Correlation between November 10-m wind-speed anomalies near Lake Challa (yellow star) (3.5°S to 3°S, 37°E to 38°E), obtained from the National Centers for Environmental Prediction (NCEP)–NCAR reanalysis (*27*) and the November Hadley Centre's HadISST1 sea surface temperature anomalies (*13*) at every grid point in the tropical Indo-Pacific from 1948 to 2011. Contours: Correlation between November precipitation anomalies at the World Meteorological Organization station 63816 in Same, Tanzania (4°05'S, 37°43'E, 872.0 m elevation), near Lake Challa and the November HadISST sea surface temperature anomalies (*13*) at every grid point from 1950 to 1989, contour interval is 0.2 and the cyan (blue dashed line) contours indicate positive (negative) correlations. The solid black line is the zero correlation contour. In November, positive wind-speed anomalies and negative precipitation anomalies near Lake Challa are significantly correlated with La Niña and negative Indian Ocean Dipole conditions at the 95% level (**B**) Time series of HadISST anomalies averaged over the western Indian Ocean from 48°E to 72°E and 24°S to 12°S (green line; 3-point running mean) (*13*) and the Niño3.4 index (red line) (*12*) show a high degree of correlation with varve thickness in Lake Challa (blue line). Thin varves correspond to El Niño events (positive Niño3.4 values) and thick varves to La Niña events (negative Niño3.4 values).

[1]Helmholtz Centre Potsdam GeoForschungsZentrum (GFZ—German Research Centre for Geosciences), Section 5.2 – Climate Dynamics and Landscape Evolution, Telegrafenberg, D-14473 Potsdam, Germany. [2]Deutsche Forschungsgemeinschaft (DFG) Graduate School 1364, University of Potsdam, Institute of Geosciences, Karl-Liebknecht Strasse 24, Haus 27, D-14476 Potsdam, Germany. [3]DFG Leibniz Center for Earth Surface Process and Climate Studies, University of Potsdam, D-14476 Potsdam, Germany. [4]Geological Institute, Department of Earth Sciences, Eidgenössische Technische Hochschule (ETH—Swiss Federal Institute of Technology), Zürich, CH-8092 Zurich, Switzerland. [5]International Pacific Research Center, School of Ocean and Earth Science and Technology, University of Hawai'i, 2525 Correa Road, HI 96822, USA. [6]Faculty of Geosciences, Utrecht University, Post Office Box 80021, 3508 TA Utrecht, Netherlands. [7]Department of Marine Organic Biogeochemistry, Nederlands Instituut voor Zeeonderzoek (NIOZ—Royal Netherlands Institute for Sea Research), Post Office Box 59, 1790 AB Den Burg, Netherlands. [8]Department of Geosciences, Princeton University, Princeton, NJ 08544, USA. [9]Lamont-Doherty Earth Observatory of Columbia University, Palisades, NY 10964–8000, USA. [10]Limnology Unit, Department of Biology, Ghent University, Ledeganckstraat 35, 9000 Gent, Belgium.

*To whom correspondence should be addressed. E-mail: gerald.haug@erdw.ethz.ch

annual cycle. It should be noted here that the varve thickness record is particularly sensitive to La Niña conditions and shows some evidence for saturation during El Niño years. The results confirm that varve thickness in Lake Challa is a robust indicator of regional climate and its large-scale sensitivities.

The correspondence between Lake Challa varve thickness and regional rainfall can also be evaluated in the more distant past by comparison with other proxies. Combined 25,000-year records of an organic biomarker [branched and isoprenoid tetraether (BIT) index] rainfall proxy from Lake Challa, as well as lake level inferred from seismic stratigraphy (*10*, *14*), show that climate in easternmost equatorial Africa was generally much drier than today between 20.5 thousand and 16.5 thousand years before the present (yr B.P.). The average varve thickness in Lake Challa is greater between ~18,500 and 21,000 yr B.P. (14.38- to 17.45-m core depth), which includes the later part of the Last Glacial Maximum [LGM, recently defined as the period 26.5 thousand to 19 thousand yr B.P., (*15*)], than in the last 3000 years (0- to 2.80-m core depth) (Fig. 2). Further, during the Maunder and Spörer sunspot minima within the Little Ice Age (A.D. 1270 to 1750), below-average varve thickness at Lake Challa coincided with high lake level in nearby Lake Naivasha (*16*). These correspondences (Fig. 2) provide evidence that a broad negative relation between the length of the windy season and rainfall also applies on time scales of centuries and millennia. Lake Challa varves primarily capture the rainfall variability that is inherently anticorrelated to local windiness (figs. S8 and S9). This type of variability dominates the interannual to decadal variability evident in instrumental data (Fig. 1A), and in general, it is associated with the regionality of atmospheric convergence (e.g., the ITCZ and its migration). The correspondences noted above between the varve thickness record and lake level and BIT index data suggest that, even on centennial to millennial time scales, a substantial part of variability in East African rainfall is driven by changes in the global and/or regional geometry of convection. In the same vein, a record from the Cariaco Basin (*17*) identifies the Little Ice Age as mostly a dry, rather than wet, interval. This out-of-phase relation between equatorial East Africa and northern South America is consistent with ENSO's global impacts on the locations of convection (*4*, *18*).

As reconstructed from the Lake Challa varve thickness record, ENSO-related interannual rainfall variability has undergone changes and transitions during the last 3000 years (Fig. 3). Our reconstruction indicates that this variability was strongly muted during the period between 300 B.C.E. and A.D. 300, in agreement with ENSO proxy data from Ecuador (*19*). An increase in variability is observed for the period AD 400 to 750. The gradual decline in variability during the Medieval Climate Anomaly terminated abruptly around A.D. 1300. A second, less prominent phase of variance reduction occurred during the Little Ice Age (A.D. 1400 to 1750). The drivers for these prominent century-scale variations are unknown.

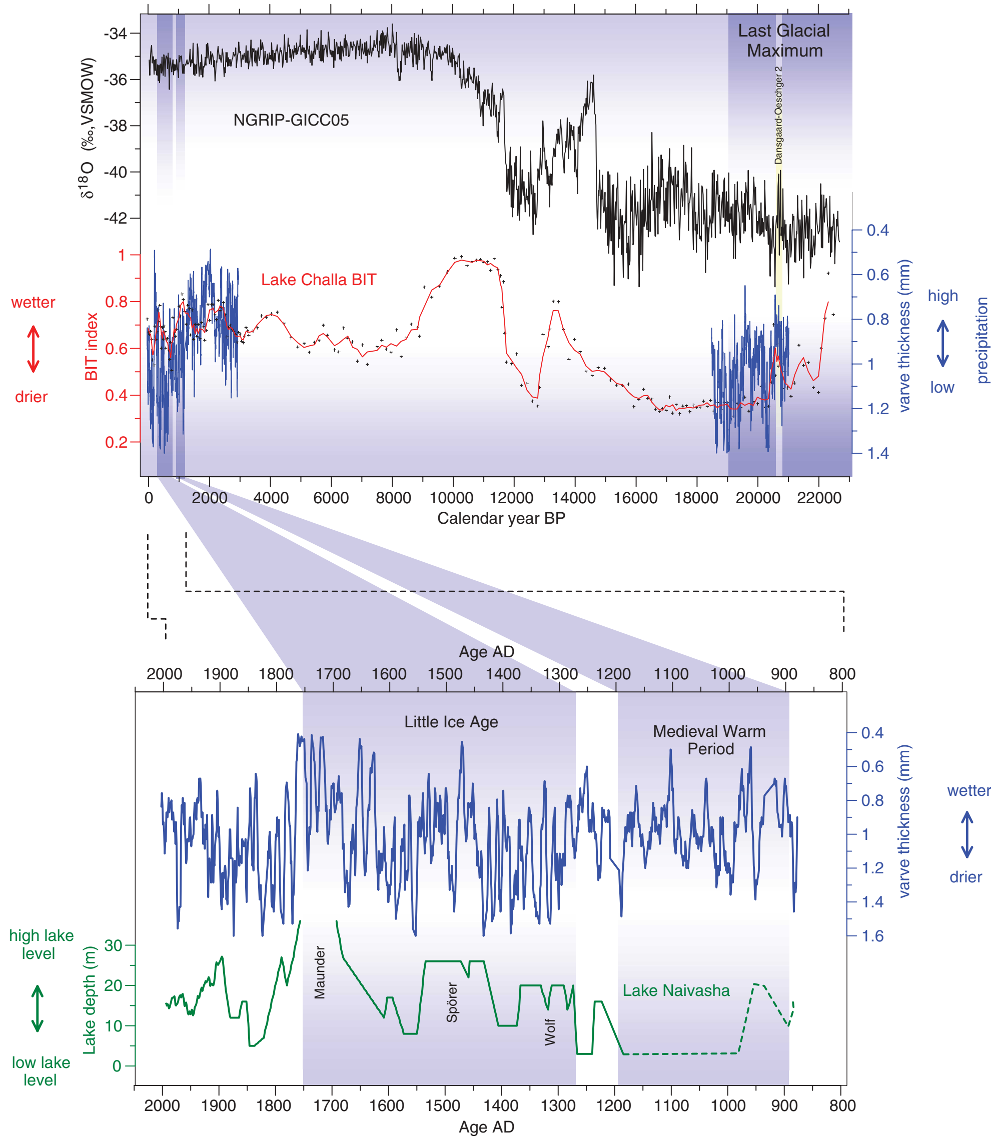


**Fig. 2.** Varve thickness data with selected other climate records spanning the last 22,500 years (top) and the past 1100 years (bottom). (**Top**) The mean varve thickness data (blue line, 21-point running mean) in comparison with the Greenland $\delta^{18}O$ ice core record on the Greenland Ice Core Chronology 2005 (GICC05) time scale [joint European Greenland Ice Core Project (NGRIP)–GICC05], (black line) (*28*); and the Lake Challa BIT-index rainfall reconstruction (red line; 3-point running mean) (*10*). The BIT index is based on the contribution of soil-derived bacterial membrane lipids relative to aquatically produced crenarchaeotal membrane lipids (*29*). (**Bottom**) Varve thickness data (blue line, 7-point running mean) during the past 1100 years compared with the lake-level record from Lake Naivasha in central Kenya (*16*) (green line).

More detailed comparisons with other ENSO-sensitive paleo-proxies may shed light on the exact role of Pacific versus Indian Ocean SST control in rainfall variability over tropical East Africa during these periods (*6*).

During the last ice age, climate in tropical Africa differed greatly from modern climate (*20*). The greater mean varve thickness in Lake Challa suggests on average stronger winds during the peak glacial climate, reminiscent of colder conditions in the western Indian Ocean (*21*). On interannual time scales, the SST anomalies in the western Indian Ocean are strongly controlled by ENSO; however, on glacial-interglacial time scales, the role of external forcings, such as reduced greenhouse gas concentrations, orbital forcing, and remote effects of the expanded ice sheets (*22*) must also be considered.

Instrumental data show that winds and rainfall are highly anticorrelated on interannual to decadal time scales (Fig. 1A and fig. S8). Thus, the use of Lake Challa varves to reconstruct rainfall variability is best justified when applied to these time scales. In this context, the interannual variability of the Lake Challa varves suggests an important difference between LGM and late Holocene conditions. The variability in varve thickness might be expected to be intrinsically related to mean varve thickness. However, although mean varve thickness in the 2554-year-long glacial section of our core is greater than in the 3056-year-long Late Holocene section, its interannual variability is markedly less (Fig. 3

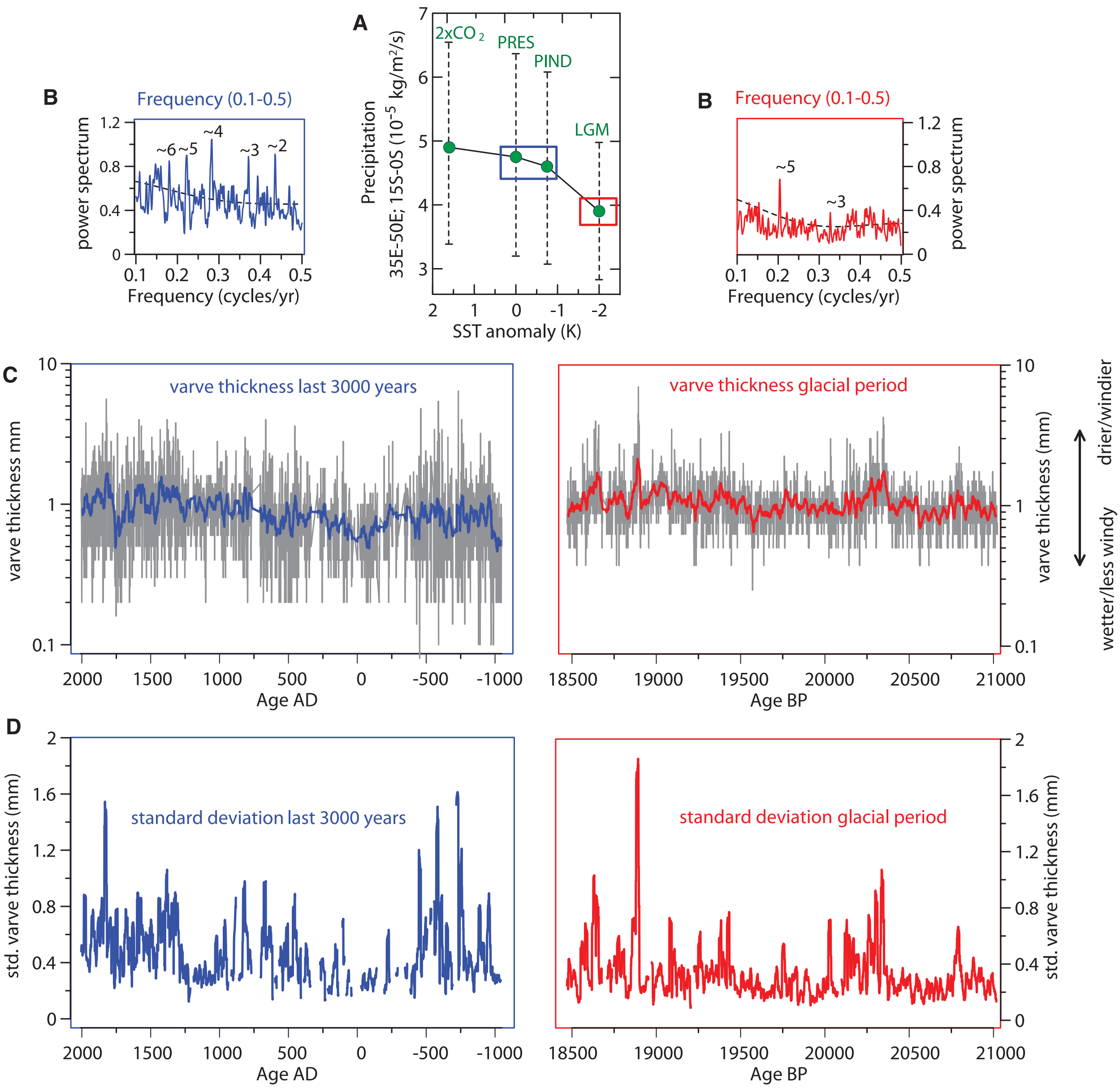


**Fig. 3.** (**A**) Simulated East African rainfall (average from 15°S to 0°S and 35°E to 50°E) and Indian Ocean surface temperature changes (average from 24°S to 12°N and 48°E to 72°E) for a series of Coupled General Circulation Model Simulations conducted with the CCSM3 climate model. The labels LGM, PIND, PRES, and $2xCO_2$ refer to the LGM experiments, the preindustrial control run, the present-day control run, and a $CO_2$-doubling experiment, respectively. The green dots represent the mean of simulated East African precipitation as a function of western Indian Ocean SST change relative to the PRES run. The vertical bars indicate the standard deviation of the simulated annual and interannual rainfall variability. Indian Ocean warming leads to an intensification of the ITCZ and increased variability. (**B**) Power spectrum on varve thickness for the last 3000 years (blue line) and between 18,500 and 21,000 yr B.P. (red line); the dashed lines represent the 95% significance level for a red noise spectrum. (**C**) Varve thickness time series for the last 3000 years and between 18,500 and 21,000 yr B.P. (gray line shows raw varve thickness data; thick blue and red lines show a 21-point running mean). (**D**) Corresponding running standard deviation for the last 3000 years and between 18,500 and 21,000 yr B.P. per 15 years.

and fig. S12). This result—less variability when varves are thicker—indicates reduced variability in East African winds and rainfall at ENSO time scales under cold LGM conditions. It is notable that the late Holocene sediments, characterized by thinner varves on average, nevertheless have the thickest individual varves (Fig. 3). Thus, although the interglacial is generally characterized by wetter, less windy conditions, it has experienced years that were windier (and thus very likely also drier) than prevailed during the last ice age (*23*).

These findings of a more interannually stable climate in East Africa during colder periods support the notion of the strong sensitivity of the winds and the hydrological cycle to the larger-scale climate. Warmer climate states appear to produce greater climate variability. This inference fits the growing consensus that current global warming will intensify the hydrological cycle, with wet regions and periods becoming wetter and dry regions and periods becoming drier (*24*). As an example of this tendency from models, experiments with the National Center for Atmospheric Research (NCAR) Community Climate Systems Model (CCSM3) coupled the general circulation model for LGM, preindustrial and modern conditions, and a doubling of preindustrial $CO_2$ levels (*25*, *26*) show the same trends in mean rainfall and rainfall variability in eastern equatorial Africa in relation to mean temperatures as indicated by our lake varve data (Fig. 3): Under warmer climates, both mean rainfall and interannual rainfall variability are greater (Fig. 3A). A future increase in the interannual variability of rainfall in equatorial eastern Africa, which is projected by the model and supported by our varve thickness data, may bring further environmental stress to a region with a reduced capacity to adapt to the mounting adverse effects of global climate change.

### References and Notes


1. M. L. Parry, Intergovernmental Panel on Climate Change Working Group II, Eds., *Climate Change 2007: Impacts, Adaptation and Vulnerability: Contribution of Working Group II to the Fourth Assessment Report of the Intergovernmental Panel on Climate Change* (Cambridge Univ. Press, Cambridge, 2007).
2. S. E. Nicholson, in *The Limnology, Climatology and Paleoclimatology of the East African Lakes*, T. C. Johnson, E. O. Odada, Eds. (Gordon & Breach, Amsterdam, 1996), pp. 25–56.
3. S. E. Nicholson, *Global Planet. Change* **26**, 137 (2000).
4. C. F. Ropelewski, M. S. Halpert, *Mon. Weather Rev.* **115**, 1606 (1987).
5. M. Latif, D. Dommenget, M. Dima, A. Grötzner, *J. Clim.* **12**, 3497 (1999).
6. L. Goddard, N. E. Graham, *J. Geophys. Res.* **104**, (D16), 19099 (1999).
7. N. H. Saji, B. N. Goswami, P. N. Vinayachandran, T. Yamagata, *Nature* **401**, 360 (1999).
8. E. Black, J. Slingo, K. R. Sperber, *Mon. Weather Rev.* **131**, 74 (2003).
9. S. Hastenrath, D. Polzin, *Q. J. R. Meteorol. Soc.* **130**, 503 (2004).
10. D. Verschuren *et al.*, *Nature* **462**, 637 (2009).
11. C. H. Pilskaln, T. C. Johnson, *Limnol. Oceanogr.* **36**, 544 (1991).
12. A. Kaplan *et al.*, *J. Geophys. Res.* **103**, (C9), 18567 (1998).
13. N. A. Rayner *et al.*, *J. Geophys. Res. Atmos.* **108**, (D14), 4407 (2003).
14. J. Moernaut *et al.*, *Earth Planet. Sci. Lett.* **290**, 214 (2010).
15. P. U. Clark *et al.*, *Science* **325**, 710 (2009).
16. D. Verschuren, K. R. Laird, B. F. Cumming, *Nature* **403**, 410 (2000).
17. G. H. Haug, K. A. Hughen, D. M. Sigman, L. C. Peterson, U. Rohl, *Science* **293**, 1304 (2001).
18. G. N. Kiladis, H. F. Diaz, *J. Clim.* **2**, 1069 (1989).
19. C. M. Moy, G. O. Seltzer, D. T. Rodbell, D. M. Anderson, *Nature* **420**, 162 (2002).
20. F. Gasse, F. Chalie, A. Vincens, M. A. J. Williams, D. Williamson, *Quat. Sci. Rev.* **27**, 2316 (2008).
21. C. Sonzogni, E. Bard, F. Rostek, *Quat. Sci. Rev.* **17**, 1185 (1998).
22. F. Justino, W. R. Peltier, *J. Clim.* **21**, 459 (2008).
23. D. McGee, W. S. Broecker, G. Winckler, *Quat. Sci. Rev.* **29**, 2340 (2010).
24. I. M. Held, B. J. Soden, *J. Clim.* **19**, 5686 (2006).
25. S. G. Yeager, C. A. Shields, W. G. Large, J. J. Hack, *J. Clim.* **19**, 2545 (2006).
26. B. L. Otto-Bliesner *et al.*, *J. Clim.* **19**, 2526 (2006).
27. E. Kalnay *et al.*, *Bull. Am. Meteorol. Soc.* **77**, 437 (1996).
28. S. O. Rasmussen *et al.*, *J. Geophys. Res. Atmos.* **111**, (D6), D06102 (2006).
29. E. C. Hopmans *et al.*, *Earth Planet. Sci. Lett.* **224**, 107 (2004).


**Acknowledgments:** This work received funding from the European Science Foundation EUROCORES program EuroCLIMATE [Framework Programme 28: Lake Challa: a Long Archive of Climate in Equatorial Africa (CHALLACEA)] and through the Graduate School GRK 1364 Shaping Earth's Surface in a Variable Environment funded by the DFG. C.W. is grateful for grant from Leibniz Center for Earth Surface Process and Climate Studies. A.T. received support from NSF grant AGS-1010869 and the Japan Agency for Marine-Earth Science and Technology (JAMSTEC). Fieldwork was conducted with research permission of the Kenyan Ministry of Education and Science to D.V. (MOEST 13/001/11C). We gratefully acknowledge C. M. Oluseno, I. Kristen, U. Frank, and A. Hoechner for comments and assistance and the CHALLACEA team for stimulating discussions. This is IPRC publication no. 805.

**Supporting Online Material**

www.sciencemag.org/cgi/content/full/333/6043/743/DC1
Materials and Methods
Figs. S1 to S12
Table S1
References

2 February 2011; accepted 17 June 2011
10.1126/science.1203724

# A 10,000-Year Record of Arctic Ocean Sea-Ice Variability—View from the Beach

Svend Funder,[1]* Hugues Goosse,[2] Hans Jepsen,[1] Eigil Kaas,[3] Kurt H. Kjær,[1] Niels J. Korsgaard,[1] Nicolaj K. Larsen,[4] Hans Linderson,[5] Astrid Lyså,[6] Per Möller,[5] Jesper Olsen,[7] Eske Willerslev[1]

We present a sea-ice record from northern Greenland covering the past 10,000 years. Multiyear sea ice reached a minimum between ~8500 and 6000 years ago, when the limit of year-round sea ice at the coast of Greenland was located ~1000 kilometers to the north of its present position. The subsequent increase in multiyear sea ice culminated during the past 2500 years and is linked to an increase in ice export from the western Arctic and higher variability of ice-drift routes. When the ice was at its minimum in northern Greenland, it greatly increased at Ellesmere Island to the west. The lack of uniformity in past sea-ice changes, which is probably related to large-scale atmospheric anomalies such as the Arctic Oscillation, is not well reproduced in models. This needs to be further explored, as it is likely to have an impact on predictions of future sea-ice distribution.

Global warming will probably cause the disappearance of summer sea ice in the Arctic Ocean during this century (*1*,*2*), and the ocean bordering North Greenland is expected to be the very last area to become ice-free in summer (*2*–*4*). We present a long-term (~10,000-year) record of variations in multiyear and land-fast sea ice from this key area, using the abundance and origin of driftwood as signals of multiyear sea ice and its traveling route, and the occurrence or absence of beach ridges as signals of seasonally open water. This record is compared with a previously published record from the western Arctic Ocean, which is based on the same type of evidence and is sensitive to the same oceanographic and climatic factors (*5*-*7*).

Driftwood on Greenland's raised beaches and shores originates from transocean drift from Asia and America. The voyage takes several

[1]Centre for GeoGenetics, Natural History Museum of Denmark, University of Copenhagen, Øster Voldgade 5-7, DK 1350 Copenhagen K, Denmark. [2]Université Catholique de Louvain, Earth and Life Institute, Centre de Recherches sur la Terre et le Climat Georges Lemaître, Chemin du Cyclotron, 2, 1348, Louvain-la-Neuve, Belgium. [3]Niels Bohr Institute, University of Copenhagen, Juliane Maries Vej 30, DK 2100 Copenhagen, Denmark. [4]Geological Institute University of Aarhus, C. F. Møllers Allé 4, DK 8000 Aarhus C, Denmark. [5]GeoBiosphere Science Centre, Quaternary Sciences, Lund University, Sölvegatan 12, SE 22362 Lund, Sweden. [6]Geological Survey of Norway, 7491 Trondheim, Norway. [7]School of Geography, Archaeology and Palaeoecology, Queen's University, Belfast, Belfast BT7 1NN, UK.

*To whom correspondence should be addressed. E-mail: svf@snm.ku.dk